Pergamon

0021-9290(95)00030-5

J. Biomechanics, Vol. 29, No. 1, pp. 91-98, 1996

0021-9290/96 $15.00 + .00

TECHNICAL NOTE

NONINVASIVE DETERMINATION OF BONE MECHANICAL PROPERTIES USING VIBRATION RESPONSE: A REFINED MODEL AND VALIDATION *IN VIVO*

S. G. Roberts,* T. M. Hutchinson,† S. B. Arnaud,† B. J. Kiratli,‡ R. B. Martin§ and C. R. Steele*

*Department of Mechanical Engineering, Stanford University, Stanford, California; †NASA Ames Research Center, Moffett Field, California; ‡Spinal Cord Injury Center, VA Medical Center, Palo Alto, California; and §Department of Orthopedics, UC Davis Medical Center, Sacramento, California, U.S.A.

Abstract—Accurate non-invasive mechanical measurement of long bones is made difficult by the masking effect of surrounding soft tissues. Mechanical response tissue analysis (MRTA) offers a method for separating the effects of the soft tissue and bone; however, a direct validation has been lacking. A theoretical analysis of wave propagation through the compressed tissue revealed a strong mass effect dependent on the relative accelerations of the probe and bone. The previous mathematical model of the bone and overlying tissue system was reconfigured to incorporate the theoretical finding. This newer model (six-parameter) was used to interpret results using MRTA to determine bone cross-sectional bending stiffness, EI_{MRTA}. The relationship between EI_{MRTA} and theoretical EI values for padded aluminum rods was $R^2 = 0.999$. A biological validation followed using monkey tibias. Each bone was tested *in vivo* with the MRTA instrument. Postmortem, the same tibias were excised and tested to failure in three-point bending to determine EI_{3-PT} and maximum load. Diaphyseal bone mineral density (BMD) measurements were also made. The relationship between EI_{3-PT} and *in vivo* EI_{MRTA} using the six-parameter model is strong ($R^2 = 0.947$) and better than that using the older model ($R^2 = 0.645$). EI_{MRTA} and BMD are also highly correlated ($R^2 = 0.853$). MRTA measurements *in vivo* and BMD *ex vivo* are both good predictors of scaled maximum strength ($R^2 = 0.915$ and $R^2 = 0.894$, respectively). This is the first biological validation of a non-invasive mechanical measurement of bone by comparison to actual values. The MRTA technique has potential clinical value for assessing long-bone mechanical properties.

Keywords: Mechanical properties; Mechanical testing; Vibration; Bone mineral; Failure; Bone stiffness.

INTRODUCTION

In order to effectively evaluate and monitor the strength and load-carrying capacity of long bones *in vivo*, an objective non-invasive measurement is desirable. Currently, bone mineral density (BMD) and bone mineral content (BMC), determined using dual-energy X-ray absorptiometry, are the state of the art clinical measures of bone integrity. The mineral mass of a bone, although essential, does not provide a complete measure of bone strength (Ott, 1993). Attempts to account for cross-sectional geometry along with bone mineral (Beck *et al.*, 1990) do not allow for variations in cross-sectional or material properties of the bone nor can they take into account the composite nature of the bone. Numerous factors influence the behavior of the bone in addition to the amount and distribution of mineralization (Carter *et al.*, 1992; Cordey *et al.*, 1992).

Martin (1991) outlined the determinants of strength and stiffness to be (i) size and shape, and (ii) mechanical properties of the composite material. Contributing to the mechanical properties of the composite material are the composition (porosity and mineralization) and organization (trabecular and cortical bone architecture, collagen fiber orientation, and amount of fatigue damage) of the tissue. The importance of these factors in determining the overall functional behavior of the long bone has been shown in a number of studies. Several researchers have found that either mineral content does not correlate well with stiffness and failure properties or that other parameters (e.g. collagen fiber orientation and texture parameters) better predict these functional properties (Currey, 1990; Martin and Ishida, 1989; Mudinger *et al.*, 1993). In order to account for all the geometric and composite material properties, there is a need for a reliable direct mechanical measurement *in vivo* of bone load-carrying capacity, as indicated by stiffness and strength.

Efforts at direct mechanical measurements of long bones have been primarily focused on vibration response techniques (Dimarogonas *et al.*, 1993; Hight *et al.*, 1980; Jurist, 1970; Young *et al.*, 1976; Van der Perre *et al.*, 1983). While much progress has been made, none of these techniques has been clinically validated nor is commonly used. A major impediment has been accounting for the effects of the soft tissue overlying the bone which can cause inconsistency in the measured response (Cornelissen *et al.*, 1986; Van der Perre *et al.*, 1983; Young *et al.*, 1979).

A vibration response method, mechanical response tissue analysis (MRTA), has shown promise for clinical application to human ulnas (McCabe *et al.*, 1991; Myburgh *et al.*, 1993, 1992). This method is particularly appealing for the clinic because the test is fast (several seconds), portable, and safe and comfortable for the patient. A low-frequency random vibration is applied transcutaneously to the mid-diaphysis of a long bone with a shaker probe, and force and acceleration of the probe are measured simultaneously. The real-time data are transformed into frequency domain and analyzed.

Received in final form 24 *February* 1995.

Address correspondence to: C. R. Steele, Ph.D., Division of Applied Mechanics, Department of Mechanical Engineering, Durand Building, Stanford University, Stanford, CA 94305, U.S.A.

The analysis method used in previously reported MRTA studies was based on a seven-parameter mathematical model of the skin and soft tissue, the surrounding musculature, and the bone (Steele *et al.*, 1988). While this method appeared to be successful in quantifying cross-sectional bending stiffness in the human ulna, it proved inadequate in tests of smaller and more flexible monkey tibias. The variation among tests *in vivo* of the same limb was unacceptably large and the fit to the response curve for individual tests was poor.

In order to improve these results, a more advanced theoretical understanding of the behavior of the soft tissue was sought. With this, a reformulation of the model and algorithm was undertaken, and the new model was validated *in vivo* using the monkey tibia.

METHODS

Model and algorithm development

The basis for the refinement of the mechanical model was an analysis of the behavior of the thin layer of soft tissue between the forcing probe and the bone. The skin and underlying tissue were assumed to be a continuous, homogeneous, incompressible, and elastic layer between the rigid test probe above and rigid bone beneath (Fig. 1). In general, the soft tissue layer has highly non-linear mechanical behavior. However, with this method, a relatively high static preload is used (8 N for human, 2–4 N for monkey), and the amplitude of vibration about the static compressed state is very small. For this case, the limiting assumption of linearity is valid (Parker *et al.*, 1990). The appropriate equation of motion in the radial direction is

$$\frac{\partial}{\partial r}(r\sigma_r) - \sigma_\theta = \rho r\ddot{u}. \tag{1}$$

The continuum and stress–strain relations for an incompressible material describe the state of stress within the thin layer.

$$\begin{aligned}\sigma_r &= \tfrac{2}{3}E\varepsilon_r - p,\\ \sigma_\theta &= \tfrac{2}{3}E\varepsilon_\theta - p,\\ \sigma_z &= \tfrac{2}{3}E\varepsilon_z - p,\\ \varepsilon_r &= \frac{1}{E}\left[\sigma_r - \nu(\sigma_\theta + \sigma_z)\right].\end{aligned} \tag{2}$$

Here $p, \sigma_r, \sigma_\theta, \sigma_z, \rho, E, \nu$ and u are the pressure, stresses in the radial, circumferential and vertical directions, density, Young's modulus, Poisson's ratio, and radial displacement, respectively, and the dots indicate differentiation with respect to time.

Strains in the radial (ε_r), circumferential (ε_θ), and vertical (ε_z) directions are related kinematically to the vertical displacement of the probe (δ).

$$\varepsilon_r = \frac{\delta}{2t}, \quad \varepsilon_\theta = \frac{\delta}{2t}, \quad \varepsilon_z = -\frac{\delta}{t}. \tag{3}$$

Balancing the driving force of the probe on the skin with the reaction force of the skin on the probe, one obtains the relation

$$F = -2\pi\int_0^a \sigma_z r\,dr. \tag{4}$$

The appropriate boundary condition for the annulus of skin, free to slip at upper and lower surfaces, at $r = a$ is approximated by acoustic impedance corresponding to an outward radiation of waves through the continuous medium.

$$\sigma_r|_{r=a} = -\rho c\dot{u}_a. \tag{5}$$

Here $\dot{u}_a$ is the velocity at $r = a$ and c is the plate velocity given by

$$c = \left(\frac{4E}{3\rho}\right)^{1/2}. \tag{6}$$

Equations (1)–(6) lead to an expression for applied force in terms of physical parameters of the tissue and acceleration, velocity, and displacement of the probe.

$$F = \left(\frac{\pi\rho a^4}{8t}\right)\ddot{\delta} + \left(\frac{\pi\rho c a^3}{2t}\right)\dot{\delta} + \left(\frac{\pi E a^2}{t}\right)\delta. \tag{7}$$

The coefficients of acceleration, velocity, and displacement in the above equation have the following physical significance in the model of the tissue layer:

$$F = m_s\ddot{\delta} + b_s\dot{\delta} + k_s\delta. \tag{8}$$

Here m_S, b_S, and k_S are the effective mass, damping, and stiffness of the soft tissue. Reasonable values of density, Young's modulus, tissue thickness, and probe radius were substituted into the coefficient terms in equation (7) and compared to typical values for the soft tissue covering human ulnas found using the mechanical response tissue analysis technique *in vivo* (Steele *et al.*, 1988).

With this improved representation of the behavior of the soft tissue, the entire physical model was modified to a six-parameter model consisting of the effective bending stiffness, damping, and mass of both the bone and soft tissue (Fig. 2). The seventh parameter present in the former model, parallel damping (b_p), has been accounted for within the soft tissue damping term (b_S) in the present formulation. Also, the inertial component of the skin mass is now dependent on the relative displacement of the probe and the bone in the plane of the forcing. The properties of the soft tissue are largely due to the displacement of, and propagation of waves through, the relatively stiff tissue compressed beneath the probe.

The six-parameter model required development of a new solution technique. Unlike the seven-parameter algorithm, a closed-form solution does not appear to be feasible because the system is overconstrained. There are still seven non-linear algebraic equations relating the physical parameters to coefficients in the polynomial transfer function, but now there are only six unknown physical parameters. Therefore, an iterative technique was developed in order to extract the mechanical properties of the bone and overlying soft tissue from the measured transfer function. This technique uses the closed-form solution of the seven-parameter model as the starting values for the iterative procedure with parallel damping and skin damping terms combined into a single effective skin damping term.

A quasi-Newton method is then used to iterate all six parameters to minimize an objective function. The objective function depends on the difference between the measured and model stiffness (F/δ) and compliance (δ/F) values at each point. Thus,

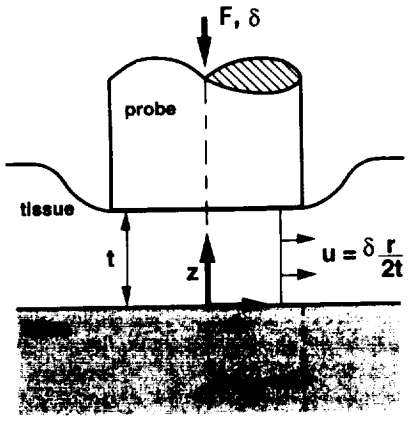

Fig. 1. The shaker probe vibrates the soft tissue and underlying bone. Waves radiate out from the center of the probe through the soft tissue. F, applied force; δ, probe displacement; a, probe radius; t, tissue thickness; u, radial displacement.

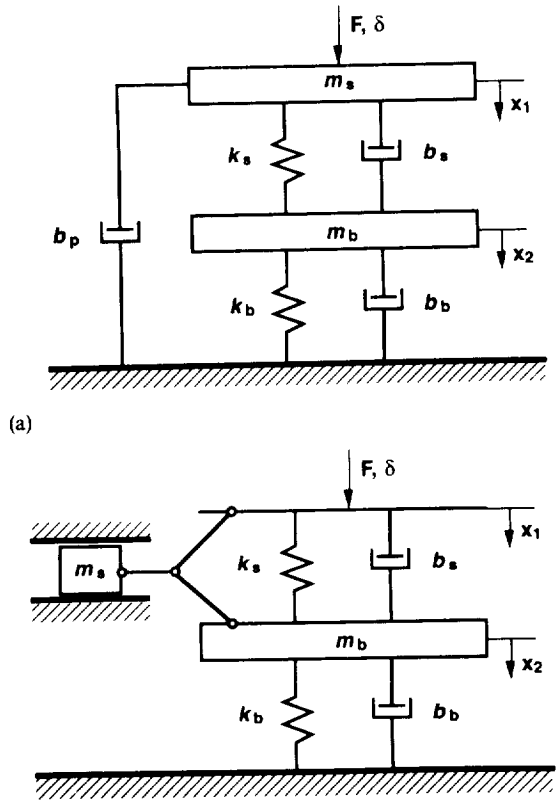

Fig. 2. (a) The seven-parameter model consists of the effective masses of the soft tissue (m_S) and bone (m_b) in series with linear springs (k_S and k_b) and viscous dash pots (b_S and b_b) and a parallel viscous dash pot (b_p) connected to the skin mass. (b) The six-parameter model consists of the effective mass of the bone (m_b) along with springs (k_S and k_b) and viscous dash pots (b_S and b_b) in series. In this new model, the motion of the effective skin mass (m_S) is a function of the difference between the displacement of the skin, x_1, and the displacement of the bone, x_2.

the objective function will be equal to zero with a perfect fit of the model response to the experimental response. More significance is given to the stiffness values in the summation because it is numerically more difficult to achieve a good fit for the stiffness curve. With the seven-parameter algorithm, a weighting function is used such that different weights can be given to different frequency ranges in formulating the objective function. With the six-parameter algorithm frequency weighting is not necessary. If the quasi-Newton method causes a change of more than 25% in the value of any one of the six parameters in one step, the step is ignored and a line search is performed in each parameter direction. The six-parameter algorithm then reverts to continuing the quasi-Newton procedure until the objective function reaches a sufficiently small value.

Method validation

The proposed changes to the physical model and algorithm did not necessitate any changes in the method or equipment used for data collection during the MRTA tests (Gait Scan, Inc., Ridgewood, NJ). The method detailed in Steele *et al.* (1988) was used. With this method, the transfer function is found from the force and acceleration responses measured at the forcing probe. The same experimental transfer function is used for both the six- and seven-parameter analysis. Because of this, it was possible to re-analyze the responses in previously reported (Steele *et al.*, 1988) tests *in vivo* of human ulnas.

As an initial validation of the six-parameter model and algorithm, MRTA tests were performed on four aluminum bars (Gait Scan, Inc.). Round aluminum bars of differing cross-sections were tested, each at least three times. A rubber pad was placed at the center of the bar to simulate the soft tissue between the probe and the specimen. These data were analyzed using both the seven-parameter and the six-parameter models and algorithms. Theoretical values of EI were calculated from the known value of Young's modulus and the radius of each bar.

A biological validation study involving 12 rhesus monkeys, *Macaca mulatta*, was completed in order to compare the abilities of the two models and algorithms to identify accurately the mechanical properties of bone and soft tissue *in vivo*. The monkey model was chosen because of its importance in many studies, including NASA space-flight. The monkeys were from two sources (UC Davis Primate Center, NASA Ames Research Center) and, due to illness, were scheduled for necropsy. The animal protocol was approved by the Animal Care and Use Committees of NASA Ames Research Center and University of California, Davis. The ages of the animals ranged from 2 to 10 yr (mean = 5.5 ± 3.1) and the body mass ranged from 2.5 to 12.7 kg (mean = 6.3 ± 3.7). The monkeys' tibial lengths (range was 0.115–0.185 m; mean = 0.153 ± 0.023) were measured *in vivo* with a metal tape from the edge of the medial condyle to the most distal edge of the medial malleolus. The accuracy of this measurement *in vivo* was confirmed postmortem by measurements of the excised tibias, also made using the metal tape. The monkeys were sedated, and each tibia was tested at least three times using the equipment manufactured for MRTA testing. The proximal and distal ends of each tibia were stiffly supported in a specially designed small animal apparatus in order to approximate the pinned–pinned end conditions assumed in the model (Hutchinson *et al.*, submitted). This apparatus provided padded clamping support from the medial, lateral, and posterior aspects of the condyle and the malleoli.

After euthanasia of the animal, each bone was excised, frozen, and later tested to failure in three-point bending on an Instron (Model 1122) machine. The frozen bones were thawed to room temperature and kept moist. Holes were drilled through the proximal and distal ends parallel to each other in the coronal plane. Surgical steel pins were inserted through these holes. Each bone was supported by these pins in a rigid frame in the same position as the MRTA tests *in vivo* such that the anterior surface was facing the crossbar, and the frame was clamped to the Instron test table (Fig. 3). The crosshead contact was centered between the pin supports. Each tibia was tested to failure in three-point bending at a displacement-controlled crosshead speed of 10 mm min^{-1}. From the strip-chart recordings of load versus displacement, the lateral bending stiffnesses were determined as the slopes in the linear region and maximum loads

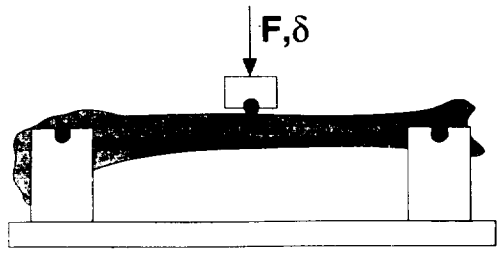

Fig. 3. The monkey tibias were supported in a pinned–pinned configuration with the crosshead centered between supports. The crosshead made contact with the anterior aspect of the bone. In the MRTA tests *in vivo*, there is the soft tissue layer between the probe and bone, musculature has significant mass and damping, and the pad end supports have little resistance to axial displacement.

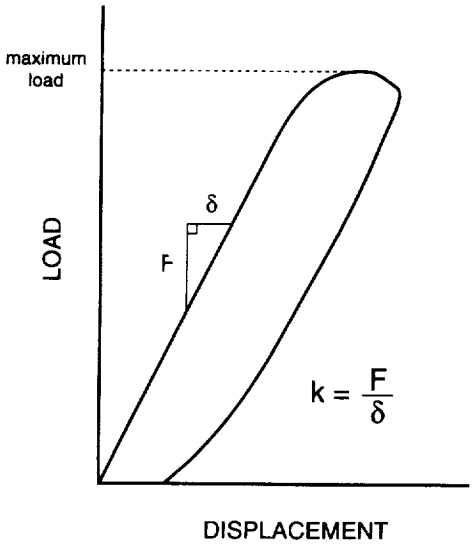

Fig. 4. The lateral bending stiffness and maximum load were determined from the load versus displacement curve for the three-point bending test of each excised monkey tibia. The lateral bending stiffness is the slope in the linear region. The curve shown was scanned in from the actual strip-chart recording.

were recorded (Fig. 4). The bones were promptly frozen for future analysis.

The lateral bending stiffness values, k_b, found using MRTA and three-point bending cannot be directly compared because the distances between supports in the two tests were different. The lateral bending stiffness values were converted into cross-sectional bending stiffness, EI, using the relation derived from elementary beam theory.

$$EI = \frac{k_b L^3}{48}. \quad (9)$$

For the bending tests, the value of length, L, was the distance between hole centers; for the MRTA tests, L was the total limb length (not the actual distance between supports).

The data from MRTA testing were processed using both the six- and seven-parameter algorithms, and the results were assessed relative to the three-point bending test results.

Significant adjustment of the weighting function was required on each individual seven-parameter analysis in order to achieve an adequate least-squares curve fit to the transfer function. For the six-parameter analysis, however, all files were batch processed at once with the number of iterations limited to 40.

Bone mineral properties were determined for both the entire bone and the middle one-third section using dual-energy X-ray absorptiometry (QDR 1000/W, Hologic Inc., Waltham, MA) in order to compare the MRTA technique to this clinically important non-invasive measurement. The excised tibias were scanned in 0.08 m of water with a 0.02 m Plexiglas base to provide a soft tissue equivalent baseline. The bones were positioned horizontally to provide an A–P view. Values of bone mineral content (BMC, in g), area of region scanned (cm^2), and areal bone mineral density (BMD, in $g\,cm^{-2}$) were obtained for all except two bones. In these bones, the mineral content appeared to be below threshold levels in the distal one-third section, and no total bone values were available; values were available for the middle one-third section. The precision of this method was high (percent coefficient of variation = 0.43%) as determined by repeated scans ($\times 4$) with repositioning performed on five bones.

The anterior–posterior and medial–lateral diameters at the center of the cleaned and excised bones were measured using digital calipers. Where there was a measurable deformation, measurements just proximal and distal to the center were averaged.

RESULTS

Theoretical values for effective mass, damping, and stiffness of the soft tissue are in good agreement with typical values measured in MRTA tests of human ulnas *in vivo* (Table 1). The effective mass is significantly larger than the actual mass of the tissue under the probe because of the large radial displacement of tissue that results from a relatively small vertical displacement of the probe, as can be seen from the kinematic expressions.

The fit of both the stiffness and flexibility response curves for all specimens using the six-parameter model and algorithm was consistently close, converging within 40 iterations in all cases and within 10 in most cases (Fig. 5). These curves include both the real and imaginary parts of the stiffness and flexibility responses. Processing in this iterative manner was, however, more time consuming than using the seven-parameter algorithm. Typically, using the six-parameter algorithm required 1–2 min to process while using the seven-parameter algorithm required 1 s to process. With very few exceptions, there was negligible change in the results using the six- vs. seven-parameter model and algorithm for the tests *in vivo* of the human ulnas.

For the tests of aluminum bars, linear regression analysis demonstrated that the value of cross-sectional bending stiffness, EI_{MRTA}, analyzed using the six-parameter model and algorithm was a strong predictor of the theoretical value, with $R^2 = 0.999$ (Fig. 6). Further, the MRTA values were within 5% of the theoretical values for all four specimens when the six-parameter model was used. A similarly good fit ($R^2 = 0.998$) was found when the seven-parameter model and algorithm were used; however, these MRTA values were only within 11% of theoretical values.

For the 21 tibia specimens included, the range of values for EI_{MRTA} *in vivo* was 2.4–22.5 $N\,m^2$ (mean = 8.5 ± 5.3). The range of values for cross-sectional bending stiffness measured in three-point bending, EI_{3-PT}, was 1.45–13.9 $N\,m^2$ (mean = 5.0 ± 3.3). Data on three monkey tibias were not included in this analysis because of difficulties with the test fixture.

Stronger relationships were found in all of the following analyses using BMD of the middle one-third section rather than of the entire tibia (compare with Roberts *et al.*, 1994). Therefore, results are presented using BMD of the middle one-third section of all bones.

There was a stronger relationship between EI determined in three-point bending and EI determined with MRTA *in vivo* when the six-parameter model and algorithm were used rather than the seven-parameter model ($R^2 = 0.947$ vs. 0.645, respec-

Table 1. Theoretical values similar to experimental values obtained in a MRTA test *in vivo* of a human ulna were found for the effective mass, damping, and stiffness of the layer of soft tissue between the test probe and the bone using equation (7). Experimental values for a group of subjects vary significantly; these given are typical for the 8 N preload. The material and geometric values for Young's modulus, density, probe radius, and tissue thickness were 4 MPa, 1000 $kg\,m^{-3}$, 5 mm, and 1 mm, respectively (Millington and Wilkinson, 1983; Parker *et al.*, 1990; Silver, 1987)

Skin parameter	Units	Theoretical	Experimental
Effective mass	g	0.245	0.239
Effective damping	$N\,s\,m^{-1}$	14.34	11.97
Effective stiffness	$kN\,m^{-1}$	314.2	322.5
Actual mass	g	0.079	NA

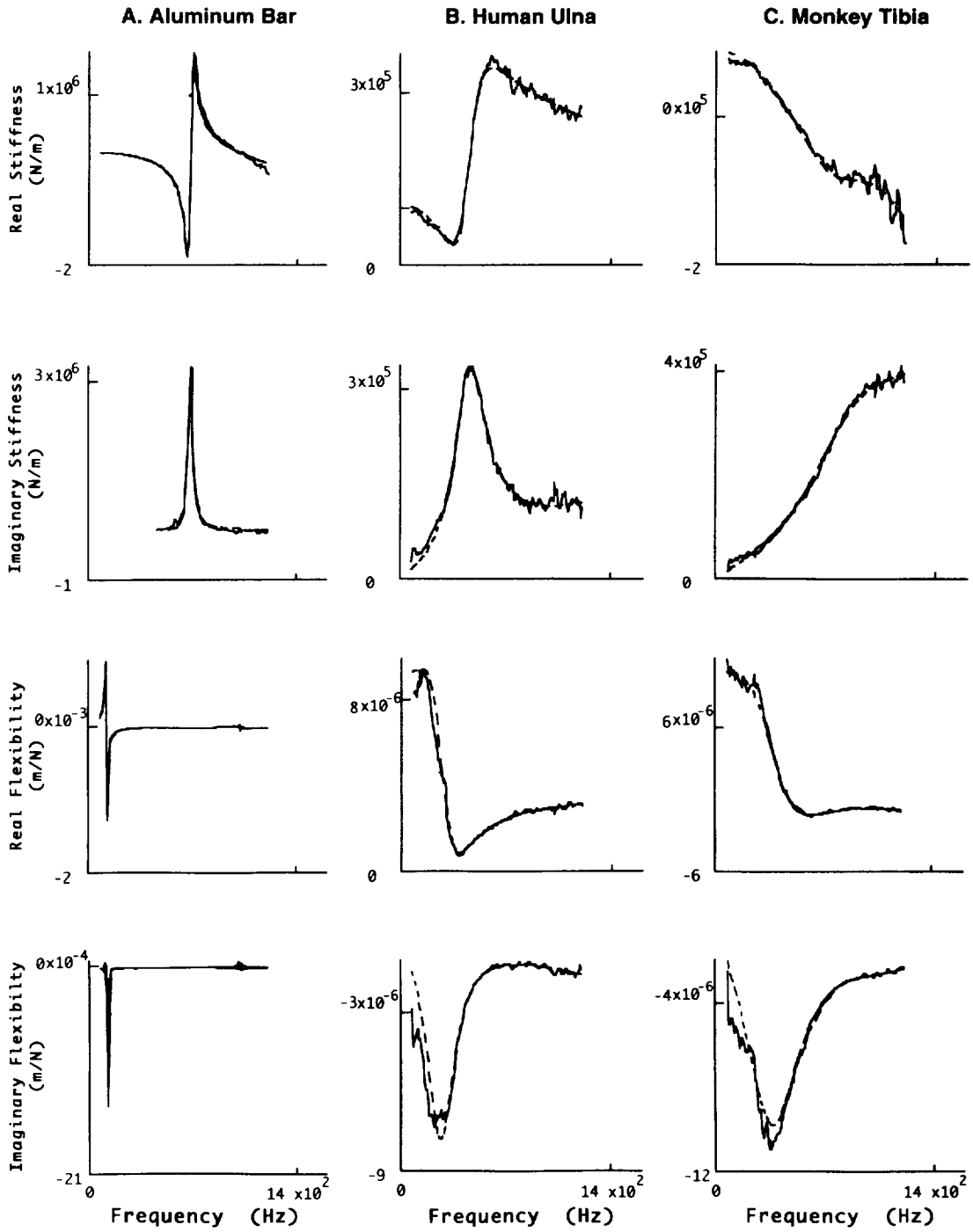

Fig. 5. Columns A, B, and C contain the real and imaginary parts of the stiffness and flexibility response curves (solid) and corresponding six-parameter curve fits (dashed) for the three specimens. The sharp peaks in the response curves of the aluminum bar are due to the relatively small damping of the bar and rubber pad. The curves of the monkey tibia are quite different from those of the other two specimens; however, the six-parameter algorithm achieves a close curve fit for all three.

tively; Fig. 7). Further, this six-parameter EI_{MRTA} displayed a better linear fit than did BMD with EI_{3-PT} ($R^2 = 0.876$; not shown).

Little difference was noted in associations between EI_{MRTA} or BMD and scaled maximum load, defined as load multiplied by pinned length and anterior-posterior diameter ($R^2 = 0.915$ and 0.894, respectively; Fig. 8). The relationship between scaled maximum load and EI_{3-PT} was very strong ($R^2 = 0.978$; not shown).

Finally, EI_{MRTA} and BMD are strongly related ($R^2 = 0.853$) (Fig. 9). All regressions are significant ($p < 0.001$).

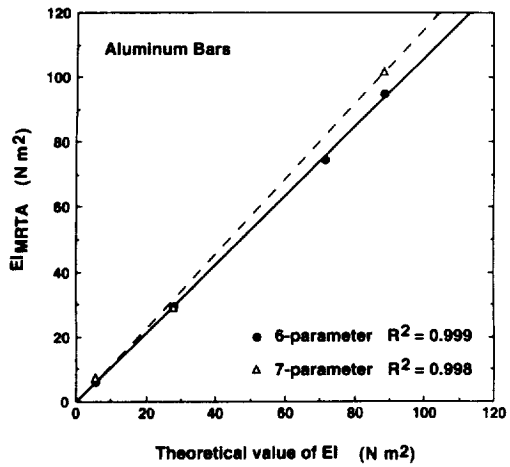

Fig. 6. The linear regressions of the six-parameter algorithm (solid line) and the seven-parameter algorithm (dashed line) on theoretically calculated values for tests on aluminum bars are presented along with the corresponding coefficients of determination. Both algorithms have very high linear regression values, but the results from the six-parameter algorithm are closer to the theoretical values.

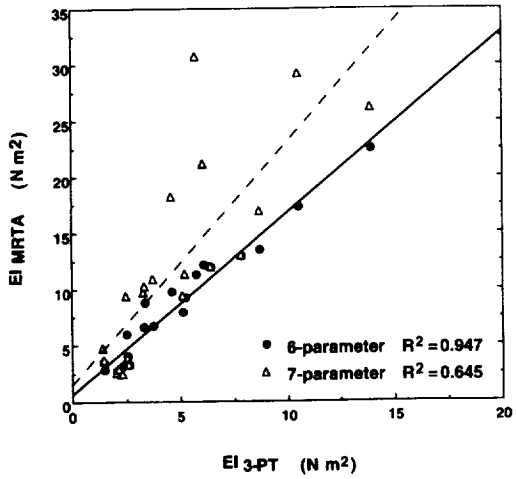

Fig. 7. The linear regressions of EI_{MRTA} analyzed using both the six-parameter (solid line) and the seven-parameter (dashed line) algorithms on EI_{3-PT} are presented along with the coefficients of determination. The relationship was much stronger for the results using the six-parameter algorithm.

DISCUSSION

The mechanical response tissue analysis technique, with the improved six-parameter model and algorithm, is a useful measurement of cross-sectional bending stiffness of long bones *in vivo*, as has been shown here for the monkey tibia. Further, this stiffness, measured with the MRTA instrument *in vivo* and the Instron *ex vivo*, is highly correlated with scaled maximum load in three-point bending ($R^2 = 0.915$ and $R^2 = 0.978$). For measurements *ex vivo*, Borders *et al.* (1977) and data from Jurist and Foltz (1977) show similar relationships between fracture moment and bending stiffness in fresh canine radii and embalmed cadaveric ulnae, respectively (Table 2). Further, as in the present study, both found stiffness to be a better predictor of failure strength than bone mineral. The reported predictive value of bone mineral measurements ranges from $R^2 = 0.15$ to $R^2 = 0.90$ (Jurist and Foltz, 1977; Myers *et al.*, 1991). Thus, it appears that EI is a more robust indicator of fracture strength because of consistently high correlations with fracture properties.

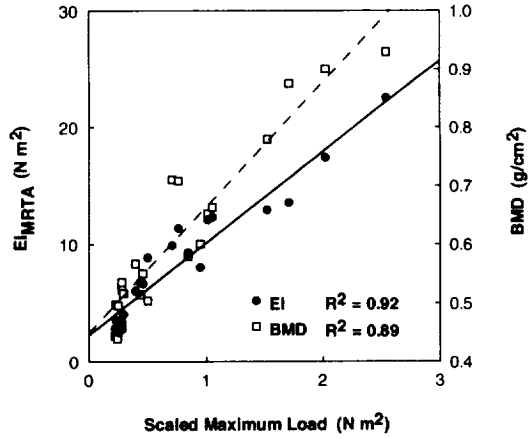

Fig. 8. The linear regressions of EI_{MRTA} *in vivo* (solid line) and BMD *ex vivo* (dashed line) on maximum load scaled by pinned length and anterior–posterior diameter are presented along with the coefficients of determination. The value of EI_{MRTA} is a better predictor of scaled maximum load than is BMD.

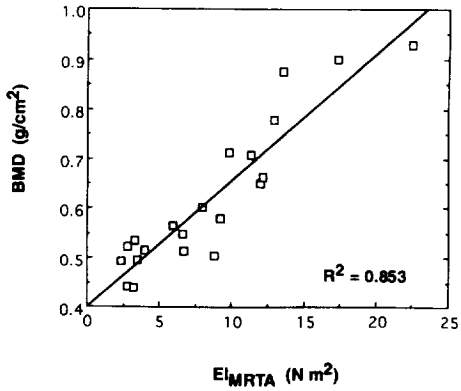

Fig. 9. The linear regression of BMD on EI_{MRTA} and the corresponding coefficient of determination are presented. The two are shown to be strongly related measures of bone integrity.

This is the first time, to the authors' knowledge, that a mechanical test of long-bone functional properties *in vivo* has been validated by direct comparison to the same property measured in a static *ex vivo* test. Modeling the bone as a simple beam appears to be valid in this frequency range where there is one significant bending mode. In the static bending tests, the maximum deflection of each bone did not exceed 15% of the outer cross-sectional diameter; it is therefore not necessary to consider any stiffening effect of the supports, and the Bernoulli–Euler beam theory is valid (Frisch-Fay, 1962). The simply supported beam model presented here assumes firm support at the proximal and distal ends of the bone. If firm support is lacking, a more complex model, incorporating additional vibration modes, would be necessary.

There is a close relationship between the results from the MRTA tests *in vivo* and three-point bending ($R^2 = 0.947$); how-

Table 2. Representative relationships between bone strength and stiffness or bone mineral illustrate the usefulness of stiffness and the inconsistency of bone mineral as indicators of structural integrity

Study	Specimen	Measurement	R^2
Borders *et al.* (1977)	Fresh canine radii	EI	0.92
		BMC	0.81
Jurist and Foltz (1977)	Embalmed cadaveric ulnae	EI	0.90
		BMC	0.88
Myers *et al.* (1991)	Frozen cadaveric radii	BMD	0.15
Geussens *et al.* (1992)	Frozen monkey radii	BMD (whole)	0.55
		BMD (diaphysis)	0.64
Present study	*In vivo* monkey tibia	EI (MRTA)	0.92
	Frozen monkey tibia	EI (Instron)	0.98
		BMD (diaphysis)	0.89

ever, values of EI_{MRTA} were approximately 60% higher than those found from Instron tests. This is attributed to the fact that, for the tests *in vivo*, total limb length was used in the calculation of cross-sectional bending stiffness. While the measurement *in vivo* of total limb length is accurate, the actual distance between the points of bone support is not known precisely because of the pad supports. Because this length term is cubed in the calculation of EI from lateral bending stiffness [equation (9)], a 10 mm central shift in the position of bone support, a physically realistic testing configuration, would account for the difference between the *in vivo* and *ex vivo* values of EI. From these results, the effective length of the tibias in the supports *in vivo* is 85% of the total limb length.

In comparisons of data analyzed using six- and seven-parameter models and algorithms, there was little distinction between the human ulna results while tremendous improvement was observed for the monkey tibias ($R^2 = 0.947$ and $R^2 = 0.645$; Fig. 7). The response curves of the two bones (Fig. 5, columns B and C) demonstrate that dynamic responses of the bone and tissue systems are quite different from one another. This difference is presumably due to the larger role played by the soft tissue in the measurement of the monkey tibia. In both human (Young *et al.*, 1976) and monkey, compressed soft tissue is effectively stiffer than the underlying long bone in bending, but the difference is greater for the smaller and more flexible monkey tibia. While soft tissue does not have a large influence on the dynamic behavior of the bone itself (Cornelissen *et al.*, 1986), the soft tissue does significantly mask the response of the underlying bone. The MRTA technique is unique among non-invasive mechanical techniques in that the behavior of the soft tissue has been modeled. Because the six-parameter model contains a more physiologically realistic representation of the soft tissue, the difference in the two models is highlighted in the monkey.

The value EI has greater physical significance than does BMD for quantifying long-bone structural integrity. In addition, it is obtained by direct mechanical measurement. Bone mineral is only one of many factors influencing the strength and other structural properties of bone. The value EI, on the other hand, is a function of the material composition, as well as the geometry and internal architecture of the bone. The importance of considering these additional properties is exemplified here in that EI is a slightly better predictor of maximum load than is BMD. Further, the bone mineral measurement was performed on the excised tibia, not *in vivo* as was the vibration test. This measurement *in vivo* of cross-sectional bending stiffness is particularly meaningful in that it provides a now proven method of evaluating and monitoring the actual structural integrity of long bones.

Acknowledgements—The authors wish to thank Michael Fourkas for his efforts in refining the algorithm and Gait Scan, Inc. for providing the equipment for the MRTA tests. We also gratefully acknowledge the support of NASA grants #199-26-12-02 and #106-30-43-04 (Cosmos) and of a National Science Foundation Graduate Fellowship to SGR.

REFERENCES

Beck, T. J., Ruff, C. B., Warden, K. E., Scott, W. W. J. and Rao, G. U. (1990) Predicting femoral neck strength from bone mineral data. A structural approach. *Invest. Radiol.* **25,** 6–18

Borders, S., Petersen, K. R. and Orne, D. (1977) Prediction of bending strength of long bones from measurements of bending stiffness and bone mineral content. *J. biomech. Engng* **99,** 40–44.

Carter, D. R., Bouxsein, M. L. and Marcus, R. (1992) New approaches for interpreting projected bone densitometry data. *J. Bone Miner. Res.* **7,** 137–145

Cordey, J., Schneider, M., Belendez, C., Ziegler, W. J., Rahn, B. A. and Perren, S. M. (1992) Effect of bone size, not density, on the stiffness of the proximal part of normal and osteoporotic human femora. *J. Bone Miner. Res.* **7** (Suppl. 2), S437–S444.

Cornelissen, P., Cornelissen, M., Van der Perre, G., Christensen, A. B., Ammitzboll, F. and Dyrbye, C. (1986) Assessment of tibial stiffness by vibration testing *in situ*—II. Influence of soft tissues, joints and fibula. *J. Biomechanics* **19,** 551–561.

Currey, J. D. (1990) Physical characteristics affecting the tensile failure properties of compact bone. *J. Biomechanics* **23,** 837–844.

Dimarogonas, A., Abbasi-Jahromi, S. and Avioli, L. (1993) Material damping for monitoring of density and strength of bones. *Calcif. Tissue Int.* **52,** 244–247.

Frisch-Fay, R. (1962) *Flexible Bars*. Butterworths, Washington.

Geusens, P., Nijs, J., Van der Perre, G., Van Audekercke, R., Lowet, G., Goovaerts, S., Barbier, A., Lacheretz, F., Remandet, B. *et al.* (1992) Longitudinal effect of tiludronate on bone mineral density, resonant frequency, and strength in monkeys. *J. Bone Miner. Res.* **7,** 599–609.

Hight, T. K., Piziali, R. L. and Nagel, D. A. (1980) Natural frequency analysis of a human tibia. *J. Biomechanics* **13,** 139–147.

Hutchinson, T. M., Bakulin, A. V., Rakhmanov, A. S., Martin, R. B., Steele, C. R. and Arnaud, S. B. Effects of chair restraint on cross-sectional bending stiffness in the tibias of Rhesus monkeys. (submitted)

Jurist, J. (1970) *In vivo* determination of the elastic response of bone. I. Method of ulnar resonant frequency determination. *Phys. Med. Biol.* **15,** 417–426.

Jurist, J. M. and Foltz, A. S. (1977) Human ulnar bending stiffness, mineral content, geometry and strength. *J. Biomechanics* **10,** 455–459.

McCabe, F., Zhou, L. J., Steele, C. R. and Marcus, R. (1991) Noninvasive assessment of ulnar bending stiffness in women. *J. Bone Miner. Res.* **6,** 53–59.

Martin, R. B. (1991) Determinants of the mechanical properties of bones. *J. Biomechanics* **24** (Suppl. 1), 79–88.

Martin, R. B. and Ishida, J. (1989) The relative effects of collagen fiber orientation, porosity, density, and mineralization on bone strength. *J. Biomechanics* **22**, 419–426.

Millington, P. F. and Wilkinson, R. (1983) *Skin* (Edited by Harrison, R. J. and McMinn, R. M. H.). Cambridge University Press, Cambridge.

Mundinger, A., Wiesmeier, B., Dinkel, E., Helwig, A., Beck, A. and Schulte Moenting, J. (1993) Quantitative image analysis of vertebral body architecture—improved diagnosis in osteoporosis based on high-resolution computed tomography. *Br. J. Radiol.* **66**, 209–213.

Myburgh, K. H., Charette, S., Zhou, L., Steele, C. R., Arnaud, S. and Marcus, R. (1993) Influence of recreational activity and muscle strength on ulnar bending stiffness in men. *Med. Sci. Sports Exerc.* **25**, 592–596.

Myburgh, K. H., Zhou, L. J., Steele, C. R., Arnaud, S. and Marcus, R. (1992) *In vivo* assessment of forearm bone mass and ulnar bending stiffness in healthy men. *J. Bone Miner. Res.* **7**, 1345–1350.

Myers, E. R., Sebeny, E. A., Hecker, A. T., Corcoran, T. A., Hipp, J. A., Greenspan, S. L. and Hayes, W. C. (1991) Correlations between photon absorption properties and failure load of the distal radius *in vitro*. *Calcif. Tissue Int.* **49**, 292–297.

Ott, S. M. (1993) When bone mass fails to predict bone failure. *Calcif. Tissue Int.* **53** (Suppl. I), S7–S13.

Parker, K. J., Huang, S. R., Musulin, R. A. and Lerner, R. M. (1990) Tissue response to mechanical vibrations for 'sonoelasticity imaging'. *Ultrasound Med. Biol.* **16**, 241–246.

Roberts, S. G., Hutchinson, T. M., Arnaud, S. B., Kiratli, B. J., Martin, R. B. and Steele, C. R. (1994) Validation of noninvasive mechanical measurement *in vivo* of bone properties. In *Proc. 2nd World Congr. of Biomechanics.* Vol. 1, p.15. Amsterdam, The Netherlands.

Silver, F. H. (1987) *Biological Materials: Structure, Mechanical Properties, and Modeling of Soft Tissues* (Edited by Welkowitz, W.) New York University Press, New York.

Steele, C. R., Zhou, L. J., Guido, D., Marcus, R., Heinrichs, W. L. and Cheema, C. (1988) Noninvasive determination of ulnar stiffness from mechanical response—*in vivo* comparison of stiffness and bone mineral content in humans. *J. biomech. Engng* **110**, 87–96.

Van der Perre, G., Van Audekercke, R., Martens, M. and Mulier, J. C (1983) Identification of *in vivo* vibration modes of human tibiae by modal analysis. *J. biomech. Engng* **105**, 244–248.

Young, D. R., Howard, W. H., Cann, C. and Steele, C. R. (1979) Noninvasive measures of bone bending rigidity in the monkey (*M. nemestrina*). *Calcif. Tissue Int.* **27**, 109–115.

Young, D. R., Thompson, G. A. and Orne, D. (1976) *In vivo* determination of mechanical properties of the human ulna by means of mechanical impedance tests: experimental results and improved mathematical model. *Med. Biol. Engng* **14**, 253–262.

NASA/CR-95-207219

Pergamon

0021-9290(95)00030-5

J. Biomechanics, Vol. 29, No. 1, pp. 91–98, 1996

0021-9290/96 $15.00 + .00

IN-52-CR

NDB

TECHNICAL NOTE

NONINVASIVE DETERMINATION OF BONE MECHANICAL PROPERTIES USING VIBRATION RESPONSE: A REFINED MODEL AND VALIDATION *IN VIVO*

S. G. Roberts,* T. M. Hutchinson,† S. B. Arnaud,† B. J. Kiratli,‡ R. B. Martin§ and C. R. Steele*

*Department of Mechanical Engineering, Stanford University, Stanford, California; †NASA Ames Research Center, Moffett Field, California; ‡Spinal Cord Injury Center, VA Medical Center, Palo Alto, California; and §Department of Orthopedics, UC Davis Medical Center, Sacramento, California, U.S.A.

Abstract—Accurate non-invasive mechanical measurement of long bones is made difficult by the masking effect of surrounding soft tissues. Mechanical response tissue analysis (MRTA) offers a method for separating the effects of the soft tissue and bone; however, a direct validation has been lacking. A theoretical analysis of wave propagation through the compressed tissue revealed a strong mass effect dependent on the relative accelerations of the probe and bone. The previous mathematical model of the bone and overlying tissue system was reconfigured to incorporate the theoretical finding. This newer model (six-parameter) was used to interpret results using MRTA to determine bone cross-sectional bending stiffness, EI_{MRTA}. The relationship between EI_{MRTA} and theoretical EI values for padded aluminum rods was $R^2 = 0.999$. A biological validation followed using monkey tibias. Each bone was tested *in vivo* with the MRTA instrument. Postmortem, the same tibias were excised and tested to failure in three-point bending to determine EI_{3-PT} and maximum load. Diaphyseal bone mineral density (BMD) measurements were also made. The relationship between EI_{3-PT} and *in vivo* EI_{MRTA} using the six-parameter model is strong ($R^2 = 0.947$) and better than that using the older model ($R^2 = 0.645$). EI_{MRTA} and BMD are also highly correlated ($R^2 = 0.853$). MRTA measurements *in vivo* and BMD *ex vivo* are both good predictors of scaled maximum strength ($R^2 = 0.915$ and $R^2 = 0.894$, respectively). This is the first biological validation of a non-invasive mechanical measurement of bone by comparison to actual values. The MRTA technique has potential clinical value for assessing long-bone mechanical properties.

Keywords: Mechanical properties; Mechanical testing; Vibration; Bone mineral; Failure; Bone stiffness.

INTRODUCTION

In order to effectively evaluate and monitor the strength and load-carrying capacity of long bones *in vivo*, an objective non-invasive measurement is desirable. Currently, bone mineral density (BMD) and bone mineral content (BMC), determined using dual-energy X-ray absorptiometry, are the state of the art clinical measures of bone integrity. The mineral mass of a bone, although essential, does not provide a complete measure of bone strength (Ott, 1993). Attempts to account for cross-sectional geometry along with bone mineral (Beck *et al.*, 1990) do not allow for variations in cross-sectional or material properties of the bone nor can they take into account the composite nature of the bone. Numerous factors influence the behavior of the bone in addition to the amount and distribution of mineralization (Carter *et al.*, 1992; Cordey *et al.*, 1992).

Martin (1991) outlined the determinants of strength and stiffness to be (i) size and shape, and (ii) mechanical properties of the composite material. Contributing to the mechanical properties of the composite material are the composition (porosity and mineralization) and organization (trabecular and cortical bone architecture, collagen fiber orientation, and amount of fatigue damage) of the tissue. The importance of these factors in determining the overall functional behavior of the long bone has been shown in a number of studies. Several researchers have found that either mineral content does not correlate well with stiffness and failure properties or that other parameters (e.g. collagen fiber orientation and texture parameters) better predict these functional properties (Currey, 1990; Martin and Ishida, 1989; Mudinger *et al.*, 1993). In order to account for all the geometric and composite material properties, there is a need for a reliable direct mechanical measurement *in vivo* of bone load-carrying capacity, as indicated by stiffness and strength.

Efforts at direct mechanical measurements of long bones have been primarily focused on vibration response techniques (Dimarogonas *et al.*, 1993; Hight *et al.*, 1980; Jurist, 1970; Young *et al.*, 1976; Van der Perre *et al.*, 1983). While much progress has been made, none of these techniques has been clinically validated nor is commonly used. A major impediment has been accounting for the effects of the soft tissue overlying the bone which can cause inconsistency in the measured response (Cornelissen *et al.*, 1986; Van der Perre *et al.*, 1983; Young *et al.*, 1979).

A vibration response method, mechanical response tissue analysis (MRTA), has shown promise for clinical application to human ulnas (McCabe *et al.*, 1991; Myburgh *et al.*, 1993, 1992). This method is particularly appealing for the clinic because the test is fast (several seconds), portable, and safe and comfortable for the patient. A low-frequency random vibration is applied transcutaneously to the mid-diaphysis of a long bone with a shaker probe, and force and acceleration of the probe are measured simultaneously. The real-time data are transformed into frequency domain and analyzed.

Received in final form 24 *February* 1995.

Address correspondence to: C. R. Steele, Ph.D., Division of Applied Mechanics, Department of Mechanical Engineering, Durand Building, Stanford University, Stanford, CA 94305, U.S.A.

The analysis method used in previously reported MRTA studies was based on a seven-parameter mathematical model of the skin and soft tissue, the surrounding musculature, and the bone (Steele *et al.*, 1988). While this method appeared to be successful in quantifying cross-sectional bending stiffness in the human ulna, it proved inadequate in tests of smaller and more flexible monkey tibias. The variation among tests *in vivo* of the same limb was unacceptably large and the fit to the response curve for individual tests was poor.

In order to improve these results, a more advanced theoretical understanding of the behavior of the soft tissue was sought. With this, a reformulation of the model and algorithm was undertaken, and the new model was validated *in vivo* using the monkey tibia.

METHODS

Model and algorithm development

The basis for the refinement of the mechanical model was an analysis of the behavior of the thin layer of soft tissue between the forcing probe and the bone. The skin and underlying tissue were assumed to be a continuous, homogeneous, incompressible, and elastic layer between the rigid test probe above and rigid bone beneath (Fig. 1). In general, the soft tissue layer has highly non-linear mechanical behavior. However, with this method, a relatively high static preload is used (8 N for human, 2–4 N for monkey), and the amplitude of vibration about the static compressed state is very small. For this case, the limiting assumption of linearity is valid (Parker *et al.*, 1990). The appropriate equation of motion in the radial direction is

$$\frac{\partial}{\partial r}(r\sigma_r) - \sigma_\theta = \rho r \ddot{u}. \tag{1}$$

The continuum and stress–strain relations for an incompressible material describe the state of stress within the thin layer.

$$\begin{aligned} \sigma_r &= \tfrac{2}{3} E\varepsilon_r - p, \\ \sigma_\theta &= \tfrac{2}{3} E\varepsilon_\theta - p, \\ \sigma_z &= \tfrac{2}{3} E\varepsilon_z - p, \\ \varepsilon_r &= \frac{1}{E}\left[\sigma_r - \nu(\sigma_\theta + \sigma_z)\right]. \end{aligned} \tag{2}$$

Here $p, \sigma_r, \sigma_\theta, \sigma_z, \rho, E, \nu$ and u are the pressure, stresses in the radial, circumferential and vertical directions, density, Young's modulus, Poisson's ratio, and radial displacement, respectively, and the dots indicate differentiation with respect to time.

Strains in the radial (ε_r), circumferential (ε_θ), and vertical (ε_z) directions are related kinematically to the vertical displacement of the probe (δ).

$$\varepsilon_r = \frac{\delta}{2t}, \quad \varepsilon_\theta = \frac{\delta}{2t}, \quad \varepsilon_z = -\frac{\delta}{t}. \tag{3}$$

Balancing the driving force of the probe on the skin with the reaction force of the skin on the probe, one obtains the relation

$$F = -2\pi \int_0^a \sigma_z r \, dr. \tag{4}$$

The appropriate boundary condition for the annulus of skin, free to slip at upper and lower surfaces, at $r = a$ is approximated by acoustic impedance corresponding to an outward radiation of waves through the continuous medium.

$$\sigma_r|_{r=a} = -\rho c \dot{u}_a. \tag{5}$$

Here $\dot{u}_a$ is the velocity at $r = a$ and c is the plate velocity given by

$$c = \left(\frac{4E}{3\rho}\right)^{1/2}. \tag{6}$$

Equations (1)–(6) lead to an expression for applied force in terms of physical parameters of the tissue and acceleration, velocity, and displacement of the probe.

$$F = \left(\frac{\pi\rho a^4}{8t}\right)\ddot{\delta} + \left(\frac{\pi\rho c a^3}{2t}\right)\dot{\delta} + \left(\frac{\pi E a^2}{t}\right)\delta. \tag{7}$$

The coefficients of acceleration, velocity, and displacement in the above equation have the following physical significance in the model of the tissue layer:

$$F = m_s\ddot{\delta} + b_s\dot{\delta} + k_s\delta. \tag{8}$$

Here m_s, b_s, and k_s are the effective mass, damping, and stiffness of the soft tissue. Reasonable values of density, Young's modulus, tissue thickness, and probe radius were substituted into the coefficient terms in equation (7) and compared to typical values for the soft tissue covering human ulnas found using the mechanical response tissue analysis technique *in vivo* (Steele *et al.*, 1988).

With this improved representation of the behavior of the soft tissue, the entire physical model was modified to a six-parameter model consisting of the effective bending stiffness, damping, and mass of both the bone and soft tissue (Fig. 2). The seventh parameter present in the former model, parallel damping (b_p), has been accounted for within the soft tissue damping term (b_s) in the present formulation. Also, the inertial component of the skin mass is now dependent on the relative displacement of the probe and the bone in the plane of the forcing. The properties of the soft tissue are largely due to the displacement of, and propagation of waves through, the relatively stiff tissue compressed beneath the probe.

The six-parameter model required development of a new solution technique. Unlike the seven-parameter algorithm, a closed-form solution does not appear to be feasible because the system is overconstrained. There are still seven non-linear algebraic equations relating the physical parameters to coefficients in the polynomial transfer function, but now there are only six unknown physical parameters. Therefore, an iterative technique was developed in order to extract the mechanical properties of the bone and overlying soft tissue from the measured transfer function. This technique uses the closed-form solution of the seven-parameter model as the starting values for the iterative procedure with parallel damping and skin damping terms combined into a single effective skin damping term.

A quasi-Newton method is then used to iterate all six parameters to minimize an objective function. The objective function depends on the difference between the measured and model stiffness (F/δ) and compliance (δ/F) values at each point. Thus,

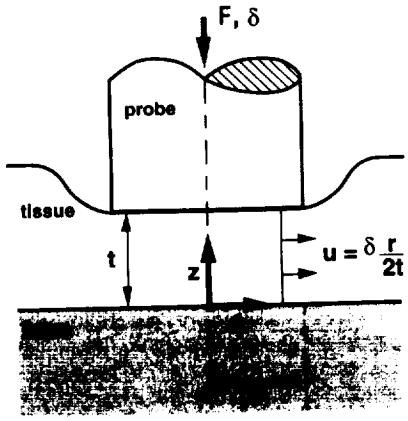

Fig. 1. The shaker probe vibrates the soft tissue and underlying bone. Waves radiate out from the center of the probe through the soft tissue. F, applied force; δ, probe displacement; a, probe radius; t, tissue thickness; u, radial displacement.

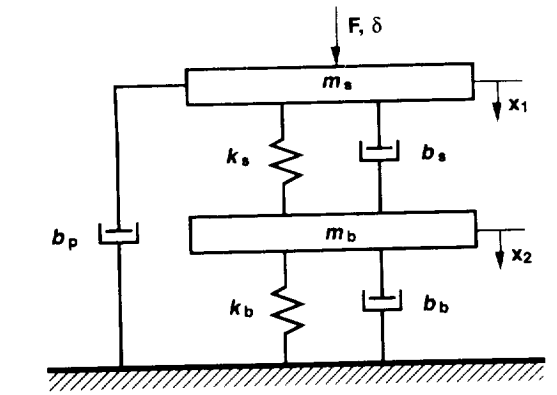

(a)

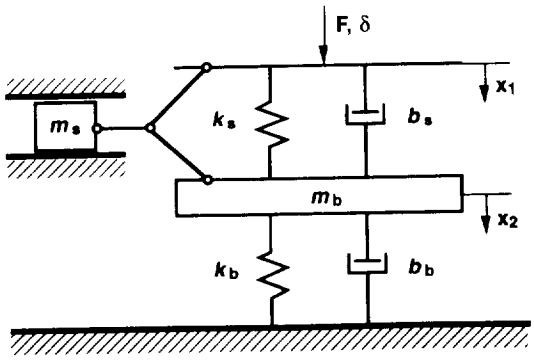

(b)

Fig. 2. (a) The seven-parameter model consists of the effective masses of the soft tissue (m_S) and bone (m_b) in series with linear springs (k_S and k_b) and viscous dash pots (b_S and b_b) and a parallel viscous dash pot (b_p) connected to the skin mass. (b) The six-parameter model consists of the effective mass of the bone (m_b) along with springs (k_S and k_b) and viscous dash pots (b_S and b_b) in series. In this new model, the motion of the effective skin mass (m_S) is a function of the difference between the displacement of the skin, x_1, and the displacement of the bone, x_2.

the objective function will be equal to zero with a perfect fit of the model response to the experimental response. More significance is given to the stiffness values in the summation because it is numerically more difficult to achieve a good fit for the stiffness curve. With the seven-parameter algorithm, a weighting function is used such that different weights can be given to different frequency ranges in formulating the objective function. With the six-parameter algorithm frequency weighting is not necessary. If the quasi-Newton method causes a change of more than 25% in the value of any one of the six parameters in one step, the step is ignored and a line search is performed in each parameter direction. The six-parameter algorithm then reverts to continuing the quasi-Newton procedure until the objective function reaches a sufficiently small value.

Method validation

The proposed changes to the physical model and algorithm did not necessitate any changes in the method or equipment used for data collection during the MRTA tests (Gait Scan, Inc., Ridgewood, NJ). The method detailed in Steele *et al.* (1988) was used. With this method, the transfer function is found from the force and acceleration responses measured at the forcing probe. The same experimental transfer function is used for both the six- and seven-parameter analysis. Because of this, it was possible to re-analyze the responses in previously reported (Steele *et al.*, 1988) tests *in vivo* of human ulnas.

As an initial validation of the six-parameter model and algorithm, MRTA tests were performed on four aluminum bars (Gait Scan, Inc.). Round aluminum bars of differing cross-sections were tested, each at least three times. A rubber pad was placed at the center of the bar to simulate the soft tissue between the probe and the specimen. These data were analyzed using both the seven-parameter and the six-parameter models and algorithms. Theoretical values of EI were calculated from the known value of Young's modulus and the radius of each bar.

A biological validation study involving 12 rhesus monkeys, *Macaca mulatta*, was completed in order to compare the abilities of the two models and algorithms to identify accurately the mechanical properties of bone and soft tissue *in vivo*. The monkey model was chosen because of its importance in many studies, including NASA space-flight. The monkeys were from two sources (UC Davis Primate Center, NASA Ames Research Center) and, due to illness, were scheduled for necropsy. The animal protocol was approved by the Animal Care and Use Committees of NASA Ames Research Center and University of California, Davis. The ages of the animals ranged from 2 to 10 yr (mean = 5.5 ± 3.1) and the body mass ranged from 2.5 to 12.7 kg (mean = 6.3 ± 3.7). The monkeys' tibial lengths (range was 0.115–0.185 m; mean = 0.153 ± 0.023) were measured *in vivo* with a metal tape from the edge of the medial condyle to the most distal edge of the medial malleolus. The accuracy of this measurement *in vivo* was confirmed postmortem by measurements of the excised tibias, also made using the metal tape. The monkeys were sedated, and each tibia was tested at least three times using the equipment manufactured for MRTA testing. The proximal and distal ends of each tibia were stiffly supported in a specially designed small animal apparatus in order to approximate the pinned–pinned end conditions assumed in the model (Hutchinson *et al.*, submitted). This apparatus provided padded clamping support from the medial, lateral, and posterior aspects of the condyle and the malleoli.

After euthanasia of the animal, each bone was excised, frozen, and later tested to failure in three-point bending on an Instron (Model 1122) machine. The frozen bones were thawed to room temperature and kept moist. Holes were drilled through the proximal and distal ends parallel to each other in the coronal plane. Surgical steel pins were inserted through these holes. Each bone was supported by these pins in a rigid frame in the same position as the MRTA tests *in vivo* such that the anterior surface was facing the crossbar, and the frame was clamped to the Instron test table (Fig. 3). The crosshead contact was centered between the pin supports. Each tibia was tested to failure in three-point bending at a displacement-controlled crosshead speed of 10 mm min^{-1}. From the strip-chart recordings of load versus displacement, the lateral bending stiffnesses were determined as the slopes in the linear region and maximum loads

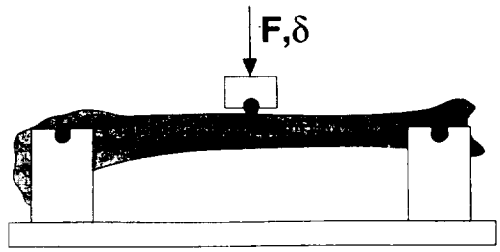

Fig. 3. The monkey tibias were supported in a pinned–pinned configuration with the crosshead centered between supports. The crosshead made contact with the anterior aspect of the bone. In the MRTA tests *in vivo*, there is the soft tissue layer between the probe and bone, musculature has significant mass and damping, and the pad end supports have little resistance to axial displacement.

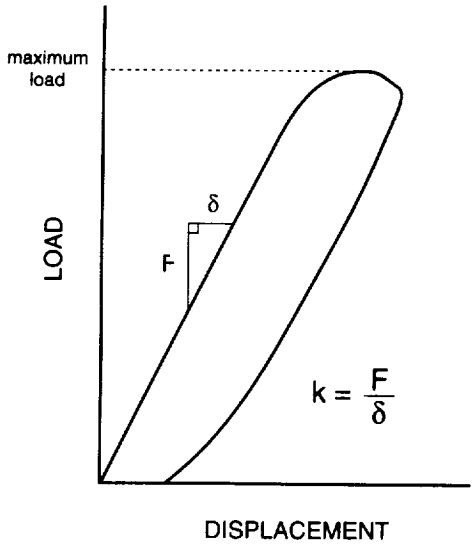

Fig. 4. The lateral bending stiffness and maximum load were determined from the load versus displacement curve for the three-point bending test of each excised monkey tibia. The lateral bending stiffness is the slope in the linear region. The curve shown was scanned in from the actual strip-chart recording.

were recorded (Fig. 4). The bones were promptly frozen for future analysis.

The lateral bending stiffness values, k_b, found using MRTA and three-point bending cannot be directly compared because the distances between supports in the two tests were different. The lateral bending stiffness values were converted into cross-sectional bending stiffness, EI, using the relation derived from elementary beam theory.

$$EI = \frac{k_b L^3}{48}. \quad (9)$$

For the bending tests, the value of length, L, was the distance between hole centers; for the MRTA tests, L was the total limb length (not the actual distance between supports).

The data from MRTA testing were processed using both the six- and seven-parameter algorithms, and the results were assessed relative to the three-point bending test results.

Significant adjustment of the weighting function was required on each individual seven-parameter analysis in order to achieve an adequate least-squares curve fit to the transfer function. For the six-parameter analysis, however, all files were batch processed at once with the number of iterations limited to 40.

Bone mineral properties were determined for both the entire bone and the middle one-third section using dual-energy X-ray absorptiometry (QDR 1000/W, Hologic Inc., Waltham, MA) in order to compare the MRTA technique to this clinically important non-invasive measurement. The excised tibias were scanned in 0.08 m of water with a 0.02 m Plexiglas base to provide a soft tissue equivalent baseline. The bones were positioned horizontally to provide an A–P view. Values of bone mineral content (BMC, in g), area of region scanned (cm^2), and areal bone mineral density (BMD, in $g\,cm^{-2}$) were obtained for all except two bones. In these bones, the mineral content appeared to be below threshold levels in the distal one-third section, and no total bone values were available; values were available for the middle one-third section. The precision of this method was high (percent coefficient of variation = 0.43%) as determined by repeated scans ($\times 4$) with repositioning performed on five bones.

The anterior–posterior and medial–lateral diameters at the center of the cleaned and excised bones were measured using digital calipers. Where there was a measurable deformation, measurements just proximal and distal to the center were averaged.

RESULTS

Theoretical values for effective mass, damping, and stiffness of the soft tissue are in good agreement with typical values measured in MRTA tests of human ulnas *in vivo* (Table 1). The effective mass is significantly larger than the actual mass of the tissue under the probe because of the large radial displacement of tissue that results from a relatively small vertical displacement of the probe, as can be seen from the kinematic expressions.

The fit of both the stiffness and flexibility response curves for all specimens using the six-parameter model and algorithm was consistently close, converging within 40 iterations in all cases and within 10 in most cases (Fig. 5). These curves include both the real and imaginary parts of the stiffness and flexibility responses. Processing in this iterative manner was, however, more time consuming than using the seven-parameter algorithm. Typically, using the six-parameter algorithm required 1–2 min to process while using the seven-parameter algorithm required 1 s to process. With very few exceptions, there was negligible change in the results using the six- vs. seven-parameter model and algorithm for the tests *in vivo* of the human ulnas.

For the tests of aluminum bars, linear regression analysis demonstrated that the value of cross-sectional bending stiffness, EI_{MRTA}, analyzed using the six-parameter model and algorithm was a strong predictor of the theoretical value, with $R^2 = 0.999$ (Fig. 6). Further, the MRTA values were within 5% of the theoretical values for all four specimens when the six-parameter model was used. A similarly good fit ($R^2 = 0.998$) was found when the seven-parameter model and algorithm were used; however, these MRTA values were only within 11% of theoretical values.

For the 21 tibia specimens included, the range of values for EI_{MRTA} *in vivo* was 2.4–22.5 $N\,m^2$ (mean = 8.5 ± 5.3). The range of values for cross-sectional bending stiffness measured in three-point bending, EI_{3-PT}, was 1.45–13.9 $N\,m^2$ (mean = 5.0 ± 3.3). Data on three monkey tibias were not included in this analysis because of difficulties with the test fixture.

Stronger relationships were found in all of the following analyses using BMD of the middle one-third section rather than of the entire tibia (compare with Roberts *et al.*, 1994). Therefore, results are presented using BMD of the middle one-third section of all bones.

There was a stronger relationship between EI determined in three-point bending and EI determined with MRTA *in vivo* when the six-parameter model and algorithm were used rather than the seven-parameter model ($R^2 = 0.947$ vs. 0.645, respec-

Table 1. Theoretical values similar to experimental values obtained in a MRTA test *in vivo* of a human ulna were found for the effective mass, damping, and stiffness of the layer of soft tissue between the test probe and the bone using equation (7). Experimental values for a group of subjects vary significantly; these given are typical for the 8 N preload. The material and geometric values for Young's modulus, density, probe radius, and tissue thickness were 4 MPa, 1000 $kg\,m^{-3}$, 5 mm, and 1 mm, respectively (Millington and Wilkinson, 1983; Parker *et al.*, 1990; Silver, 1987)

Skin parameter	Units	Theoretical	Experimental
Effective mass	g	0.245	0.239
Effective damping	$N\,s\,m^{-1}$	14.34	11.97
Effective stiffness	$kN\,m^{-1}$	314.2	322.5
Actual mass	g	0.079	NA

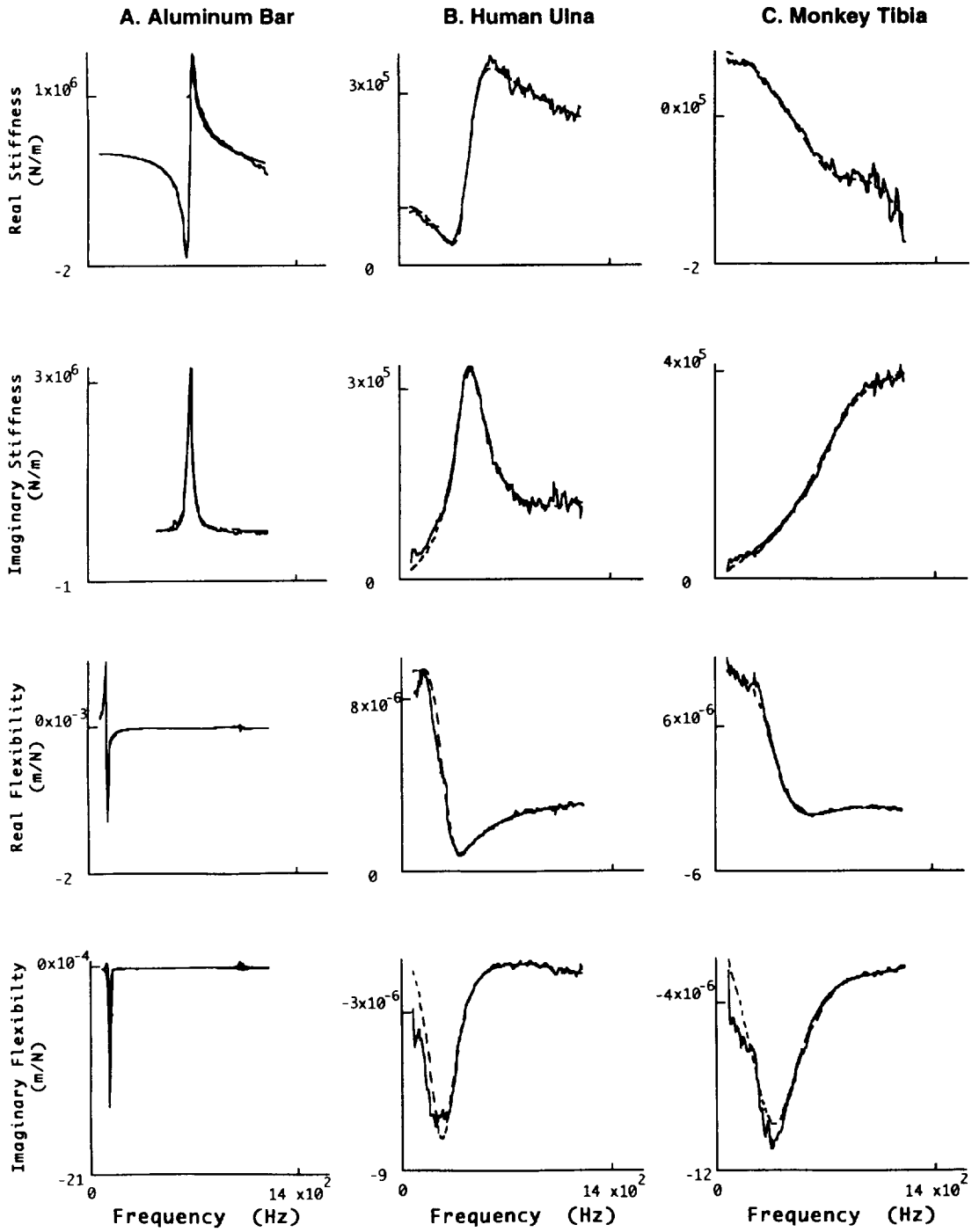

Fig. 5. Columns A, B, and C contain the real and imaginary parts of the stiffness and flexibility response curves (solid) and corresponding six-parameter curve fits (dashed) for the three specimens. The sharp peaks in the response curves of the aluminum bar are due to the relatively small damping of the bar and rubber pad. The curves of the monkey tibia are quite different from those of the other two specimens; however, the six-parameter algorithm achieves a close curve fit for all three.

tively; Fig. 7). Further, this six-parameter EI_{MRTA} displayed a better linear fit than did BMD with EI_{3-PT} ($R^2 = 0.876$; not shown).

Little difference was noted in associations between EI_{MRTA} or BMD and scaled maximum load, defined as load multiplied by pinned length and anterior–posterior diameter ($R^2 = 0.915$ and 0.894, respectively; Fig. 8). The relationship between scaled maximum load and EI_{3-PT} was very strong ($R^2 = 0.978$; not shown).

Finally, EI_{MRTA} and BMD are strongly related ($R^2 = 0.853$) (Fig. 9). All regressions are significant ($p < 0.001$).

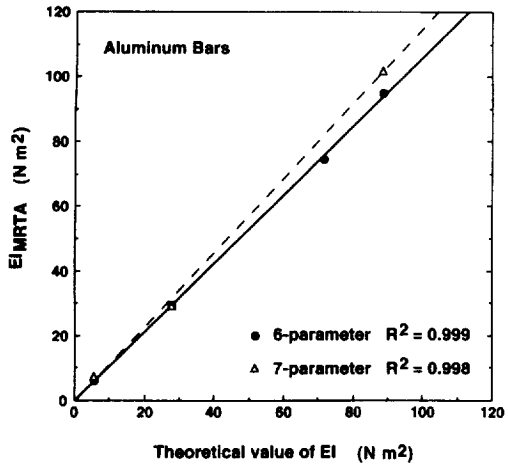

Fig. 6. The linear regressions of the six-parameter algorithm (solid line) and the seven-parameter algorithm (dashed line) on theoretically calculated values for tests on aluminum bars are presented along with the corresponding coefficients of determination. Both algorithms have very high linear regression values, but the results from the six-parameter algorithm are closer to the theoretical values.

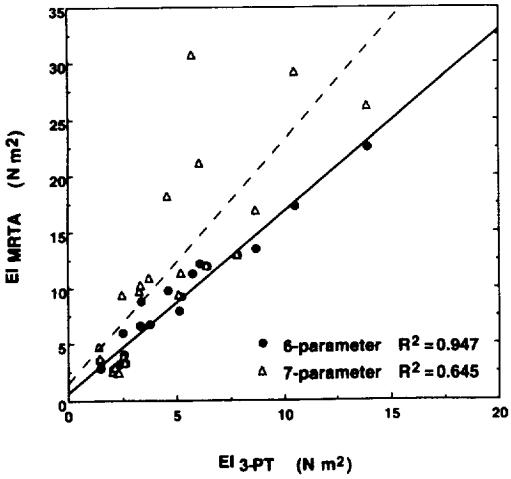

Fig. 7. The linear regressions of EI_{MRTA} analyzed using both the six-parameter (solid line) and the seven-parameter (dashed line) algorithms on EI_{3-PT} are presented along with the coefficients of determination. The relationship was much stronger for the results using the six-parameter algorithm.

DISCUSSION

The mechanical response tissue analysis technique, with the improved six-parameter model and algorithm, is a useful measurement of cross-sectional bending stiffness of long bones *in vivo*, as has been shown here for the monkey tibia. Further, this stiffness, measured with the MRTA instrument *in vivo* and the Instron *ex vivo*, is highly correlated with scaled maximum load in three-point bending ($R^2 = 0.915$ and $R^2 = 0.978$). For measurements *ex vivo*, Borders *et al.* (1977) and data from Jurist and Foltz (1977) show similar relationships between fracture moment and bending stiffness in fresh canine radii and embalmed cadaveric ulnae, respectively (Table 2). Further, as in the present study, both found stiffness to be a better predictor of failure strength than bone mineral. The reported predictive value of bone mineral measurements ranges from $R^2 = 0.15$ to $R^2 = 0.90$ (Jurist and Foltz, 1977; Myers *et al.*, 1991). Thus, it appears that EI is a more robust indicator of fracture strength because of consistently high correlations with fracture properties.

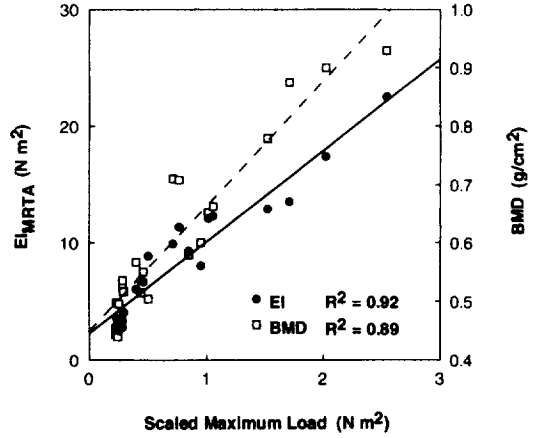

Fig. 8. The linear regressions of EI_{MRTA} *in vivo* (solid line) and BMD *ex vivo* (dashed line) on maximum load scaled by pinned length and anterior–posterior diameter are presented along with the coefficients of determination. The value of EI_{MRTA} is a better predictor of scaled maximum load than is BMD.

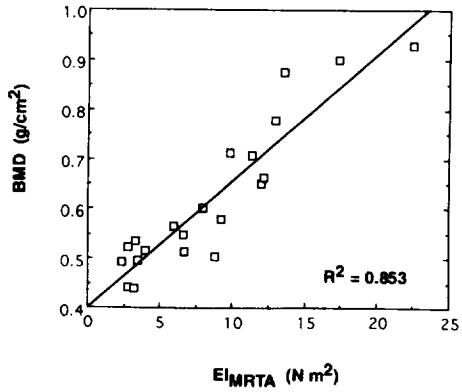

Fig. 9. The linear regression of BMD on EI_{MRTA} and the corresponding coefficient of determination are presented. The two are shown to be strongly related measures of bone integrity.

This is the first time, to the authors' knowledge, that a mechanical test of long-bone functional properties *in vivo* has been validated by direct comparison to the same property measured in a static *ex vivo* test. Modeling the bone as a simple beam appears to be valid in this frequency range where there is one significant bending mode. In the static bending tests, the maximum deflection of each bone did not exceed 15% of the outer cross-sectional diameter; it is therefore not necessary to consider any stiffening effect of the supports, and the Bernoulli–Euler beam theory is valid (Frisch-Fay, 1962). The simply supported beam model presented here assumes firm support at the proximal and distal ends of the bone. If firm support is lacking, a more complex model, incorporating additional vibration modes, would be necessary.

There is a close relationship between the results from the MRTA tests *in vivo* and three-point bending ($R^2 = 0.947$); how-

Table 2. Representative relationships between bone strength and stiffness or bone mineral illustrate the usefulness of stiffness and the inconsistency of bone mineral as indicators of structural integrity

Study	Specimen	Measurement	R^2
Borders *et al.* (1977)	Fresh canine radii	EI	0.92
		BMC	0.81
Jurist and Foltz (1977)	Embalmed cadaveric ulnae	EI	0.90
		BMC	0.88
Myers *et al.* (1991)	Frozen cadaveric radii	BMD	0.15
Geussens *et al.* (1992)	Frozen monkey radii	BMD (whole)	0.55
		BMD (diaphysis)	0.64
Present study	*In vivo* monkey tibia	EI (MRTA)	0.92
	Frozen monkey tibia	EI (Instron)	0.98
		BMD (diaphysis)	0.89

ever, values of EI_{MRTA} were approximately 60% higher than those found from Instron tests. This is attributed to the fact that, for the tests *in vivo*, total limb length was used in the calculation of cross-sectional bending stiffness. While the measurement *in vivo* of total limb length is accurate, the actual distance between the points of bone support is not known precisely because of the pad supports. Because this length term is cubed in the calculation of EI from lateral bending stiffness [equation (9)], a 10 mm central shift in the position of bone support, a physically realistic testing configuration, would account for the difference between the *in vivo* and *ex vivo* values of EI. From these results, the effective length of the tibias in the supports *in vivo* is 85% of the total limb length.

In comparisons of data analyzed using six- and seven-parameter models and algorithms, there was little distinction between the human ulna results while tremendous improvement was observed for the monkey tibias ($R^2 = 0.947$ and $R^2 = 0.645$; Fig. 7). The response curves of the two bones (Fig. 5, columns B and C) demonstrate that dynamic responses of the bone and tissue systems are quite different from one another. This difference is presumably due to the larger role played by the soft tissue in the measurement of the monkey tibia. In both human (Young *et al.*, 1976) and monkey, compressed soft tissue is effectively stiffer than the underlying long bone in bending, but the difference is greater for the smaller and more flexible monkey tibia. While soft tissue does not have a large influence on the dynamic behavior of the bone itself (Cornelissen *et al.*, 1986), the soft tissue does significantly mask the response of the underlying bone. The MRTA technique is unique among non-invasive mechanical techniques in that the behavior of the soft tissue has been modeled. Because the six-parameter model contains a more physiologically realistic representation of the soft tissue, the difference in the two models is highlighted in the monkey.

The value EI has greater physical significance than does BMD for quantifying long-bone structural integrity. In addition, it is obtained by direct mechanical measurement. Bone mineral is only one of many factors influencing the strength and other structural properties of bone. The value EI, on the other hand, is a function of the material composition, as well as the geometry and internal architecture of the bone. The importance of considering these additional properties is exemplified here in that EI is a slightly better predictor of maximum load than is BMD. Further, the bone mineral measurement was performed on the excised tibia, not *in vivo* as was the vibration test. This measurement *in vivo* of cross-sectional bending stiffness is particularly meaningful in that it provides a now proven method of evaluating and monitoring the actual structural integrity of long bones.

Acknowledgements—The authors wish to thank Michael Fourkas for his efforts in refining the algorithm and Gait Scan, Inc. for providing the equipment for the MRTA tests. We also gratefully acknowledge the support of NASA grants #199-26-12-02 and #106-30-43-04 (Cosmos) and of a National Science Foundation Graduate Fellowship to SGR.

REFERENCES

Beck, T. J., Ruff, C. B., Warden, K. E., Scott, W. W. J. and Rao, G. U. (1990) Predicting femoral neck strength from bone mineral data. A structural approach. *Invest. Radiol.* **25,** 6–18

Borders, S., Petersen, K. R. and Orne, D. (1977) Prediction of bending strength of long bones from measurements of bending stiffness and bone mineral content. *J. biomech. Engng* **99,** 40–44.

Carter, D. R., Bouxsein, M. L. and Marcus, R. (1992) New approaches for interpreting projected bone densitometry data. *J. Bone Miner. Res.* **7,** 137–145

Cordey, J., Schneider, M., Belendez, C., Ziegler, W. J., Rahn, B. A. and Perren, S. M. (1992) Effect of bone size, not density, on the stiffness of the proximal part of normal and osteoporotic human femora. *J. Bone Miner. Res.* **7** (Suppl. 2), S437–S444.

Cornelissen, P., Cornelissen, M., Van der Perre, G., Christensen, A. B., Ammitzboll, F. and Dyrbye, C. (1986) Assessment of tibial stiffness by vibration testing *in situ*—II. Influence of soft tissues, joints and fibula. *J. Biomechanics* **19,** 551–561.

Currey, J. D. (1990) Physical characteristics affecting the tensile failure properties of compact bone. *J. Biomechanics* **23,** 837–844.

Dimarogonas, A., Abbasi-Jahromi, S. and Avioli, L. (1993) Material damping for monitoring of density and strength of bones. *Calcif. Tissue Int.* **52,** 244–247.

Frisch-Fay, R. (1962) *Flexible Bars.* Butterworths, Washington.

Geusens, P., Nijs, J., Van der Perre, G., Van Audekercke, R., Lowet, G., Goovaerts, S., Barbier, A., Lacheretz, F., Remandet, B. *et al.* (1992) Longitudinal effect of tiludronate on bone mineral density, resonant frequency, and strength in monkeys. *J. Bone Miner. Res.* **7,** 599–609.

Hight, T. K., Piziali, R. L. and Nagel, D. A. (1980) Natural frequency analysis of a human tibia. *J. Biomechanics* **13,** 139–147.

Hutchinson, T. M., Bakulin, A. V., Rakhmanov, A. S., Martin, R. B., Steele, C. R. and Arnaud, S. B. Effects of chair restraint on cross-sectional bending stiffness in the tibias of Rhesus monkeys. (submitted)

Jurist, J. (1970) *In vivo* determination of the elastic response of bone. I. Method of ulnar resonant frequency determination. *Phys. Med. Biol.* **15,** 417–426.

Jurist, J. M. and Foltz, A. S. (1977) Human ulnar bending stiffness, mineral content, geometry and strength. *J. Biomechanics* **10,** 455–459.

McCabe, F., Zhou, L. J., Steele, C. R. and Marcus, R. (1991) Noninvasive assessment of ulnar bending stiffness in women. *J. Bone Miner. Res.* **6,** 53–59.

Martin, R. B. (1991) Determinants of the mechanical properties of bones. *J. Biomechanics* **24** (Suppl. 1), 79–88.

Martin, R. B. and Ishida, J. (1989) The relative effects of collagen fiber orientation, porosity, density, and mineralization on bone strength. *J. Biomechanics* **22,** 419–426.

Millington, P. F. and Wilkinson, R. (1983) *Skin* (Edited by Harrison, R. J. and McMinn, R. M. H.). Cambridge University Press, Cambridge.

Mundinger, A., Wiesmeier, B., Dinkel, E., Helwig, A., Beck, A. and Schulte Moenting, J. (1993) Quantitative image analysis of vertebral body architecture—improved diagnosis in osteoporosis based on high-resolution computed tomography. *Br. J. Radiol.* **66,** 209–213.

Myburgh, K. H., Charette, S., Zhou, L., Steele, C. R., Arnaud, S. and Marcus, R. (1993) Influence of recreational activity and muscle strength on ulnar bending stiffness in men. *Med. Sci. Sports Exerc.* **25,** 592–596.

Myburgh, K. H., Zhou, L. J., Steele, C. R., Arnaud, S. and Marcus, R. (1992) *In vivo* assessment of forearm bone mass and ulnar bending stiffness in healthy men. *J. Bone Miner. Res.* **7,** 1345–1350.

Myers, E. R., Sebeny, E. A., Hecker, A. T., Corcoran, T. A., Hipp, J. A., Greenspan, S. L. and Hayes, W. C. (1991) Correlations between photon absorption properties and failure load of the distal radius *in vitro*. *Calcif. Tissue Int.* **49,** 292–297.

Ott, S. M. (1993) When bone mass fails to predict bone failure. *Calcif. Tissue Int.* **53** (Suppl. I), S7–S13.

Parker, K. J., Huang, S. R., Musulin, R. A. and Lerner, R. M. (1990) Tissue response to mechanical vibrations for 'sonoelasticity imaging'. *Ultrasound Med. Biol.* **16,** 241–246.

Roberts, S. G., Hutchinson, T. M., Arnaud, S. B., Kiratli, B. J., Martin, R. B. and Steele, C. R. (1994) Validation of noninvasive mechanical measurement *in vivo* of bone properties. In *Proc. 2nd World Congr. of Biomechanics.* Vol. 1, p.15. Amsterdam, The Netherlands.

Silver, F. H. (1987) *Biological Materials: Structure, Mechanical Properties, and Modeling of Soft Tissues* (Edited by Welkowitz, W.) New York University Press, New York.

Steele, C. R., Zhou, L. J., Guido, D., Marcus, R., Heinrichs, W. L. and Cheema, C. (1988) Noninvasive determination of ulnar stiffness from mechanical response—*in vivo* comparison of stiffness and bone mineral content in humans. *J. biomech. Engng* **110,** 87–96.

Van der Perre, G., Van Audekercke, R., Martens, M. and Mulier, J. C (1983) Identification of *in vivo* vibration modes of human tibiae by modal analysis. *J. biomech. Engng* **105,** 244–248.

Young, D. R., Howard, W. H., Cann, C. and Steele, C. R. (1979) Noninvasive measures of bone bending rigidity in the monkey (*M. nemestrina*). *Calcif. Tissue Int.* **27,** 109–115.

Young, D. R., Thompson, G. A. and Orne, D. (1976) *In vivo* determination of mechanical properties of the human ulna by means of mechanical impedance tests: experimental results and improved mathematical model. *Med. Biol. Engng* **14,** 253–262.